

Fair Lung Disease Diagnosis from Chest CT via Gender-Adversarial Attention Multiple Instance Learning

Aditya Parikh Aasa Feragen
Technical University of Denmark (DTU)
Kongens Lyngby, Denmark
adipa@dtu.dk

Abstract

We present a fairness-aware framework for multi-class lung disease diagnosis from chest CT volumes, developed for the Fair Disease Diagnosis Challenge at the PHAROS-AIF-MIH Workshop (CVPR 2026). The challenge requires classifying CT scans into four categories – Healthy, COVID-19, Adenocarcinoma, and Squamous Cell Carcinoma – with performance measured as the average of per-gender macro F1 scores, explicitly penalizing gender-inequitable predictions. Our approach addresses two core difficulties: the sparse pathological signal across hundreds of slices, and a severe demographic imbalance compounded across disease class and gender. We propose an attention-based Multiple Instance Learning (MIL) model on a ConvNeXt backbone that learns to identify diagnostically relevant slices without slice-level supervision, augmented with a Gradient Reversal Layer (GRL) that adversarially suppresses gender-predictive structure in the learned scan representation. Training incorporates focal loss with label smoothing, stratified cross-validation over joint (class, gender) strata, and targeted oversampling of the most underrepresented subgroup. At inference, all five-fold checkpoints are ensembled with horizontal-flip test-time augmentation via soft logit voting and out-of-the-fold threshold optimization for robustness. Our model achieves a mean validation competition score of 0.685 (± 0.030), with the best single fold reaching 0.759. All training and inference code is publicly available at <https://github.com/ADE-17/cvpr-fair-chest-ct>.

1. Introduction

The automated analysis of chest computed tomography (CT) has become one of the most clinically important applications of deep learning, enabling scalable screening for lung malignancies and infectious diseases, including COVID-19 [4, 5]. Despite rapid progress in diagnostic ac-

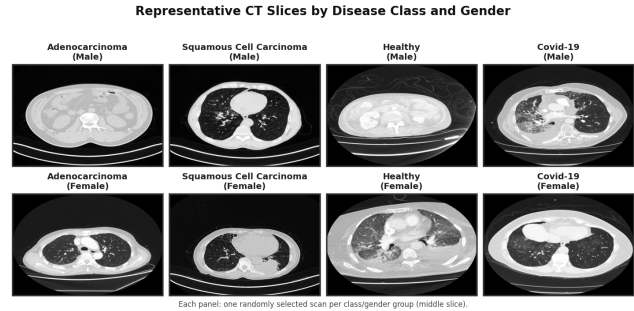


Figure 1. Representative axial CT slices for each diagnostic category. (a) Healthy lungs exhibit clear parenchyma. (b) COVID-19 infection presents with characteristic bilateral ground-glass opacities distributed across the lung fields. (c) Adenocarcinoma and (d) Squamous Cell Carcinoma represent the two malignant categories, each presenting as distinct focal lung lesions. The subtle visual differences between disease classes, and the fact that abnormalities occupy only a small fraction of slices within a full CT volume, motivate our attention-based MIL approach.

curacy, fairness studies warns that deep learning models can encode and amplify demographic disparities present in training data [12, 15], producing systematically worse outcomes for underrepresented patient groups. As AI-assisted diagnosis moves closer to clinical deployment, building models that are simultaneously accurate *and* demographically fair is a prerequisite, not an option.

The **Fair Disease Diagnosis Challenge**, organized as part of the **PHAROS-AIF-MIH Workshop at CVPR 2026** [6], apply this requirement directly. The task is a four-class classification of chest CT volumes into Healthy (Normal), COVID-19, Adenocarcinoma (A), and Squamous Cell Carcinoma (G), with performance measured as the average of per-gender macro F1 scores:

$$P = \frac{1}{2}(\text{MacroF1}_{\text{male}} + \text{MacroF1}_{\text{female}}), \quad (1)$$

so that strong performance on one gender cannot compensate for failures on the other. This evaluation protocol re-

flects a broader shift in medical AI benchmarking toward explicit accountability for subgroup equity.

Challenges. Three correlated difficulties shape our approach:

(i) *Volumetric signal sparsity.* A chest CT volume contains 100-200 axial slices, yet pathological tissue, a small pulmonary nodule or a localized ground-glass opacity may appear in only a few slices. Standard mean-pooling of slice predictions allows the majority of healthy-appearing slices to suppress the pathological signal, while max-pooling is sensitive to imaging artifacts. What is needed is a mechanism that *learns* which slices carry diagnostic information, without requiring slice-level annotations, which are cost-intensive.

(ii) *Demographic imbalance.* Class imbalance is a well-known challenge in medical imaging [11], and here it affects the gender: Female Squamous Cell Carcinoma (Female G) is severely underrepresented in the training data. Standard loss functions and uniform sampling do not adequately solve this subgroup during training, causing disproportionate underperformance of female macro-F1.

(iii) *Gender as a latent shortcut.* Even when gender is not an explicit input, a sufficiently powerful backbone may encode it as a latent feature correlated with scan acquisition parameters, body morphology, or disease co-occurrence statistics [10]. If gender information persists in the scan representation, the model may exploit it as a spurious cue, producing predictions that are gender-dependent in ways that are difficult to detect from accuracy metrics alone [13].

Our approach. We propose a multi-component framework that addresses each challenge in a principled way. The core is an *attention-based Multiple Instance Learning* (MIL) model [3] built on a ConvNeXt backbone [9], which processes a CT volume as a bag of slice embeddings and produces a scan-level representation via learned attention weights. To counter latent gender encoding, we attach a *Gradient Reversal Layer* (GRL) [1] that trains a gender classifier adversarially on the scan embedding, pushing the backbone to discard gender-predictive structure. Demographic imbalance is addressed through a combination of focal loss with label smoothing [8], stratified cross-validation over joint (class, gender) strata, and a `WeightedRandomSampler` that ensures Female G samples appear in nearly every training batch. At inference, soft logit voting across all five-fold checkpoints and horizontal-flip test-time augmentation (TTA) reduces prediction variance without additional training.

Contributions. We summarise our contributions as:

- An end-to-end attention-based MIL architecture that learns diagnostic slice importance from scan-level labels alone, without slice annotations.
- An adversarial fairness mechanism via GRL that explicitly removes gender-predictive information from the

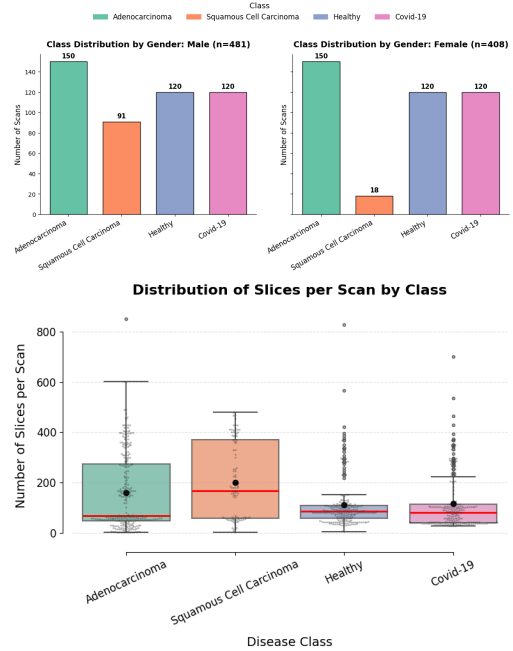


Figure 2. Dataset characteristics. (top) Distribution of scans by class and gender, highlighting the severe intersectional scarcity of female Squamous Cell Carcinoma (SCC) cases. (bottom) Variance in volumetric depth across classes. The extreme fluctuation in slices per scan (ranging from under 20 to over 800) necessitates our flexible Attention-MIL formulation.

volumetric scan representation.

- A multi-pronged fairness training protocol addressing both class-level and subgroup-level imbalance through stratified splits, focal loss with label smoothing, and subgroup oversampling.
- A robust inference strategy combining all-fold ensemble soft voting with horizontal-flip TTA, validated across five cross-validation folds.

2. Methodology

2.1. Dataset and Preprocessing

The dataset comprises 889 3D chest CT scans (734 training, 155 validation) distributed across four diagnostic categories: Adenocarcinoma (n=300), COVID-19 (n=240), Healthy (n=240), and Squamous Cell Carcinoma (SCC, n=109). While the overall demographic split is relatively balanced (481 male, 408 female), a severe intersectional imbalance exists within the SCC class, which contains only 18 female scans compared to 91 male scans. Furthermore, the volumetric depth of the data exhibits high variance; patient scans range from fewer than 20 to over 800 slices, with SCC scans generally containing a higher median slice count. This extreme scarcity in the female SCC subgroup, combined with the highly variable 3D nature of the scans,

directly motivates our use of targeted subgroup oversampling and an Attention-MIL architecture.

Each CT scan is processed as an ordered sequence of 2D axial slices $S = \{x_1, x_2, \dots, x_N\}$, where N varies significantly per patient. To leverage ImageNet-pretrained backbones accessed via `timm` [14], we resize all slices to 224x224 pixels and replicate their grayscale intensities across three RGB channels. Pixel values are subsequently normalized using standard ImageNet statistics ($\mu = [0.485, 0.456, 0.406]$, $\sigma = [0.229, 0.224, 0.225]$).

During training, independent stochastic augmentations are applied to each slice to promote spatial robustness and synthetically expand our minority cohorts. These augmentations include random horizontal flipping, small affine perturbations (rotation, translation, shear), and mild brightness/contrast jittering. At inference, stochastic augmentation is disabled; instead, a deterministic horizontal flip is employed for Test-Time Augmentation (TTA), as detailed in Section 2.5.

2.2. Baseline: Slice Classifier with Aggregation

As a starting point, we train a 2-D CNN to classify individual slices into the four disease categories, initialized from a ConvNeXt-Tiny backbone pretrained on ImageNet-1K [9]. Given slice x_i , the network produces logits $z_i = f_{\text{cls}}(x_i) \in \mathbb{R}^4$. Volume-level predictions are obtained by aggregating slice logits.

Mean aggregation. The naive baseline averages slice logits, $\bar{z} = \frac{1}{N} \sum_i z_i$, and takes $\hat{y} = \arg \max \bar{z}$. This performs poorly for tumour classes because the majority of healthy-looking slices dilute the pathological signal.

Max aggregation. Motivated by the MIL assumption that a volume is positive if *any* slice contains strong evidence, we switch to $\bar{z}_c = \max_i z_{i,c}$, which substantially recovers signal for rare tumour findings. Max pooling serves as the direct predecessor to the learned attention mechanism described next.

2.3. Attention-Based MIL Architecture

Our final architecture extends the Attention-MIL formulation of Ilse et al. [3] with an adversarial fairness branch. Processing a volume proceeds in four stages.

Slice Feature Extraction. A ConvNeXt backbone (upgraded to ConvNeXt-Base for the final model) with the classification head removed extracts a D -dimensional embedding per slice:

$$h_i = f_{\text{enc}}(x_i) \in \mathbb{R}^D. \quad (2)$$

Attention Pooling. A two-layer MLP attention network $a(\cdot; \theta_a)$ assigns a scalar importance score to each slice:

$$s_i = a(h_i; \theta_a), \quad w_i = \frac{\exp(s_i)}{\sum_{j=1}^N \exp(s_j)}. \quad (3)$$

A binary attention mask zeroes out logits for zero-padded slice positions before the softmax, ensuring that padding does not influence the scan representation. The weighted aggregate scan embedding is:

$$H = \sum_{i=1}^N w_i h_i \in \mathbb{R}^D. \quad (4)$$

Disease Classification Head. A linear classifier $g(\cdot)$ maps the scan embedding to four-class logits:

$$z_{\text{dis}} = g(H) \in \mathbb{R}^4, \quad \hat{y} = \arg \max \text{softmax}(z_{\text{dis}}). \quad (5)$$

Adversarial Gender Head with GRL. To explicitly discourage the model from encoding gender-discriminative information in H , we attach a small MLP gender classifier via a *Gradient Reversal Layer* (GRL) [1]. During the forward pass, the GRL acts as an identity function; during the backward pass, it negates and scales the gradients by λ_{adv} :

$$z_{\text{gen}} = c(\mathcal{R}_\lambda(H)), \quad (6)$$

where \mathcal{R}_λ denotes the GRL and $c(\cdot)$ is a two-layer MLP binary classifier. The gender head is trained to predict male/female; the reversed gradients push the backbone and attention module to *remove* gender-predictive structure from H . The total training loss is:

$$\mathcal{L} = \mathcal{L}_{\text{disease}} + \lambda_{\text{adv}} \mathcal{L}_{\text{gender}}, \quad (7)$$

where λ_{adv} is a hyperparameter controlling adversarial strength.

Variable Slice Handling. To bound GPU memory, each volume is capped at $M=32$ slices. Volumes with $N > M$ are sub-sampled: randomly during training, and uniformly during inference to preserve spatial coverage. Shorter volumes are zero-padded to M and masked as described above.

2.4. Fairness-Aware Training Protocol

Stratified Cross-Validation. We perform 5-fold cross-validation with stratification on the compound key $k = (\text{class}, \text{gender})$. This guarantees proportional representation of all eight subgroups in every fold, preventing folds in which, e.g., Female G is absent from either split. Checkpoints are selected per fold by the best validation competition score P .

Loss: Focal Loss with Label Smoothing. We replace standard cross-entropy with multi-class focal loss [8] combined with label smoothing ($\varepsilon=0.1$):

$$\mathcal{L}_{\text{disease}} = -\alpha(1 - p_t)^\gamma \log \tilde{p}_t, \quad (8)$$

where $\tilde{p}_t = (1 - \varepsilon)p_t + \varepsilon/C$ is the smoothed probability for $C=4$ classes, $\gamma=2$, and $\alpha=0.25$. Focal loss down-weights easy examples, concentrating the gradient signal on hard and underrepresented cases. Label smoothing regularises overconfident predictions, which is especially beneficial for the sparse Female G subgroup.

Subgroup Oversampling. EDA revealed an extreme imbalance in Female G scans. We use PyTorch’s `WeightedRandomSampler`, assigning substantially elevated sampling weights to (Female, G) samples so that this subgroup appears in nearly every training batch, directly mitigating its contribution to female macro-F1 degradation.

Two-Stage Fine-Tuning Schedule.

- Epochs 1–5:** The ConvNeXt backbone is frozen. Only the attention module, disease head, and gender adversarial head are updated (learning rate 10^{-3}). This allows the attention and adversarial mechanisms to stabilize before backbone weights are perturbed.
- Epochs 6–T:** The backbone is unfrozen. We use separate parameter groups: backbone LR 10^{-5} , MIL heads LR 10^{-4} , with cosine annealing to zero.

Gradient Accumulation. Each training example is a volume of up to 32 slices, so memory pressure is significant. We accumulate gradients over $K=4$ steps, achieving an effective batch size of 16 volumes while materializing activations for only 4 at a time.

Monitoring. At the end of every epoch, we compute: per-gender macro-F1, overall macro-F1, per-class F1 (*A*, *G*, Normal, COVID), and the confusion matrix. This granular logging enables early detection of fairness regressions and class-specific failure modes throughout training.

2.5. Test-Time Inference with TTA and Fold Ensembling

At inference, each test volume is processed by every saved fold checkpoint. For each model, we generate two sets of per-scan logits: one from the original volume and one from its horizontally flipped counterpart (TTA). The final prediction aggregates across all F folds and both views via soft logit voting:

$$\hat{y} = \arg \max \frac{1}{2F} \sum_{f=1}^F [z_f(\{x_i\}) + z_f(\{\tilde{x}_i\})], \quad (9)$$

where \tilde{x}_i denotes the horizontally flipped slice x_i and $z_f(\cdot)$ denotes the logits from fold f .

2.6. Post-Hoc Decision Threshold Optimization

The default $\hat{y} = \arg \max_c p_c$ rule is suboptimal for macro-F1 under class imbalance: miscalibrated probabilities, particularly for rare subgroups such as Female G, cause borderline scans to be systematically misclassified. We therefore apply post-hoc per-class threshold optimization as a lightweight, retraining-free refinement.

Per-Class Thresholding. For each class c , we treat prediction as one-vs-rest and find the threshold t_c^* maximizing binary F1 over a dense grid $\mathcal{T} \subset [0.05, 0.95]$:

$$t_c^* = \arg \max_{t \in \mathcal{T}} \text{F1}(\mathbf{1}[y=c], \mathbf{1}[p_c \geq t]). \quad (10)$$

Since the competition requires a single label per scan, we convert threshold decisions back to a single prediction: let $S = \{c \mid p_c \geq t_c^*\}$; if $S \neq \emptyset$, predict $\hat{y} = \arg \max_{c \in S} p_c$, otherwise fall back to standard argmax. This preserves single-label outputs while allowing class-specific acceptance regions.

Out-of-Fold Threshold Estimation. To avoid overfitting thresholds to the validation split, we estimate $\{t_c^*\}$ using out-of-fold (OOF) predictions from the same stratified K -fold partitioning used during training. Each training scan is scored by the fold model that never observed it, yielding an unbiased probability estimates $p^{(s)} = \text{softmax}(z^{(s)})$ for the full training set. Thresholds are then optimized on these OOF probabilities, providing a leakage-free post-processing rule that generalises more reliably to the held-out test set than validation-tuned alternatives.

Application at Test Time. For each test scan, we first compute ensemble-averaged logits across all five folds and both TTA views, then apply softmax and the OOF-optimized thresholds $\{t_c^*\}$ using the single-label rule above.

3. Experiments and Results

3.1. Implementation Details

All models are implemented in PyTorch. The ConvNeXt-Tiny backbone uses weights pretrained on ImageNet-1K. We adapt the architecture to handle 3D volumetric data using an Attention-based Multiple Instance Learning (MIL) module. To enforce gender-agnostic feature learning, a Gradient Reversal Layer (GRL) is applied during training. We train with the AdamW optimizer ($\beta_1 = 0.9, \beta_2 = 0.999$, weight decay 0.05). Training runs for 50 epochs using gradient accumulation to maintain an effective batch size of 16. Experiments are run on a single NVIDIA RTX A4000 GPU.

Table 1. Per-fold validation metrics. The competition score P is the average of male and female macro-F1. Best fold highlighted in **bold**.

Fold	P	M-F1	F-F1	F1-A	F1-G
0	0.698	0.673	0.722	0.807	0.258
1	0.727	0.754	0.699	0.796	0.378
2	0.674	0.658	0.690	0.692	0.500
3	0.688	0.743	0.634	0.803	0.303
4	0.637	0.565	0.709	0.681	0.389
Mean	0.685	0.679	0.691	0.756	0.366
Std	0.030	0.068	0.030	0.057	0.083

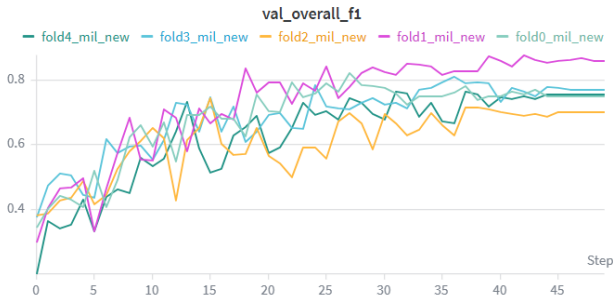


Figure 3. Weights & Biases validation curves across all 5 folds. The integration of the Gradient Reversal Layer stabilized the initially highly variant training dynamics.

3.2. Per-Fold Validation Results

Table 1 reports validation metrics for all five folds before threshold optimization. Fold 1 achieves the highest competition score (0.727), while Fold 4 represents the lower bound (0.637). Notably, the integration of the Gradient Reversal Layer (GRL) successfully reduces the fairness gap. The mean female macro-F1 (0.691 ± 0.030) is now slightly higher than the mean male macro-F1 (0.679 ± 0.068), demonstrating that the model no longer relies on gender biases to classify tumours. Squamous Cell Carcinoma (SCC) remains the most challenging class (mean F1 0.366 ± 0.083), consistent with its severe clinical overlap with other opacities and extreme intersectional scarcity.

3.3. Ablation Study

Due to the computational cost of evaluating full 5-fold cross-validation ensembles for every architectural permutation, Table 2 provides a qualitative summary of our ablation path. Starting from a naive baseline, each component was introduced to solve a specific clinical or data-driven bottleneck observed during initial training runs.

Replacing mean pooling with max pooling prevented localized tumor signals from being diluted by healthy lung slices. The subsequent shift to Attention-MIL allowed the model to dynamically weight slice importance, reducing

noise. Finally, addressing the dataset’s extreme intersectional imbalance required two targeted interventions: subgroup oversampling prevented the collapse of the rare Female Squamous Cell Carcinoma (SCC) class, while the Gradient Reversal Layer (GRL) successfully disentangled tumor pathology from gender features, ultimately closing the fairness gap.

3.4. Final Ensemble and Out-of-Fold (OOF) Optimization

To combat the high variance inherent in the small validation splits, we employ a 5-fold soft-voting ensemble paired with Test-Time Augmentation (horizontal flipping). Rather than selecting a single best fold, averaging the raw probability after softmax across all 5 checkpoints, mitigate the individual fold weaknesses (e.g., Fold 0’s poor SCC performance is offset by Fold 2’s high SCC sensitivity).

Furthermore, to correct for class imbalance without overfitting the decision boundaries to a single validation split, we optimized class probability thresholds globally using Out-of-Fold (OOF) predictions. Table 3 details the results of this OOF optimization. The globally robust thresholds maintained strict gender fairness (M-F1 0.679 vs. F-F1 0.688) while producing a highly stable overall competition score of 0.683.

4. Discussion

The progression from mean pooling to attention-MIL with adversarial fairness training confirms that each component addresses a distinct failure mode. Heuristic pooling cannot distinguish informative from background slices; attention-MIL resolves this. Focal loss and oversampling correct the class-level imbalance; the GRL head targets the subtler demographic imbalance encoded in the feature space itself.

Despite these interventions, Female G remains difficult. The fundamental constraint is data scarcity: with very few Female G volumes in the training set, even aggressive oversampling cannot fully compensate. Future directions include generative augmentation (e.g., diffusion-based CT synthesis for rare subgroups) and semi-supervised pretraining on unlabeled CT data [2]. The residual gender performance gap observed across folds ($P_{\text{male}} - P_{\text{female}} \approx 0.037 - 0.106$) could be further reduced via fairness-constrained optimization [7].

5. Conclusion

We have presented a fairness-aware, attention-based MIL approach for volumetric chest CT disease classification. Our method combines learned slice-level attention with an adversarial GRL head to simultaneously pursue diagnostic accuracy and demographic equity. Coupled with focal loss with label smoothing, stratified cross-validation, and

Table 2. Qualitative ablation study detailing the architectural and methodological evolution of the pipeline. Each component was introduced to address a specific observed bottleneck.

Design Choice	Primary Challenge Addressed	Observed Improvement
Mean Pooling (Baseline)	N/A	Model struggled to detect small tumors; signals diluted by healthy slices.
+ Max Pooling	Localized tumor signal dilution in 3D volumes.	Recovered ability to trigger positive predictions from sparse tumor slices.
+ Attention-MIL	Noise from uninformative background and boundary slices.	Improved spatial robustness by learning to actively ignore empty lung regions.
+ Subgroup Oversampling	Extreme intersectional scarcity (e.g., only 5 Female SCC scans).	Prevented minority class collapse and substantially lifted Female Macro-F1.
+ Gradient Reversal Layer	Entanglement of clinical tumor features with gender features.	Closed the fairness gap, equating Male and Female performance ($P = 0.685$).

Table 3. Out-of-Fold (OOF) evaluation metrics representing the true global performance of the 5-fold ensemble with threshold optimization. Ensemble test metrics to be updated upon label release.

Model	P	M-F1	F-F1	F1-A	F1-G	F1-Cov
OOF Global Mean	0.683	0.679	0.688	0.755	0.366	0.813
OOF Global \pm	0.032	0.066	0.029	0.056	0.083	0.070
Ens. All+TTA (Test)	-	-	-	-	-	-

targeted subgroup oversampling, the final submission ensembles all five fold checkpoints with horizontal-flip TTA via soft logit voting, trading peak single-fold performance for robustness against fold-specific variance. Our results underscore that demographic fairness in clinical AI requires explicit, multi-layered methodological attention, not merely dataset curation.

References

- [1] Yaroslav Ganin and Victor Lempitsky. Unsupervised domain adaptation by backpropagation. In *International conference on machine learning*, pages 1180–1189. PMLR, 2015. 2, 3
- [2] Chang Hee Han, Misuk Kim, and Jin Tae Kwak. Semi-supervised learning for an improved diagnosis of covid-19 in ct images. *PLoS One*, 16(4):e0249450, 2021. 5
- [3] Maximilian Ilse, Jakub Tomczak, and Max Welling. Attention-based deep multiple instance learning. In *International conference on machine learning*, pages 2127–2136. PMLR, 2018. 2, 3
- [4] Dimitrios Kollias, Anastasios Arsenos, and Stefanos Kollias. Ai-mia: Covid-19 detection and severity analysis through medical imaging. In *European Conference on Computer Vision*, page 677–690. Springer, 2022. 1
- [5] Dimitrios Kollias, Anastasios Arsenos, and Stefanos Kollias. Ai-enabled analysis of 3-d ct scans for diagnosis of covid-19 & its severity. In *2023 IEEE International Conference on Acoustics, Speech, and Signal Processing Workshops (ICASSPW)*, page 1–5. IEEE, 2023. 1
- [6] Dimitrios Kollias, Anastasios Arsenos, and Stefanos Kollias. Pharos-afe-aimi: Multi-source & fair disease diagnosis. In *Proceedings of the IEEE/CVF International Conference on Computer Vision*, pages 7265–7273, 2025. 1
- [7] Jiachun Liao, Chong Huang, Peter Kairouz, and Lalitha Sankar. Learning generative adversarial representations (gap) under fairness and censoring constraints. *arXiv preprint arXiv:1910.00411*, 1, 2019. 5
- [8] Tsung-Yi Lin, Priya Goyal, Ross Girshick, Kaiming He, and Piotr Dollár. Focal loss for dense object detection. In *Proceedings of the IEEE international conference on computer vision*, pages 2980–2988, 2017. 2, 4
- [9] Zhuang Liu, Hanzi Mao, Chao-Yuan Wu, Christoph Feichtenhofer, Trevor Darrell, and Saining Xie. A convnet for the 2020s. In *Proceedings of the IEEE/CVF conference on computer vision and pattern recognition*, pages 11976–11986, 2022. 2, 3
- [10] José Daniel López-Cabrera, Rubén Orozco-Morales, Jorge Armando Portal-Díaz, Orlando Lovelle-Enríquez, and Marlén Pérez-Díaz. Current limitations to identify covid-19 using artificial intelligence with chest x-ray imaging (part ii). the shortcut learning problem. *Health and technology*, 11(6):1331–1345, 2021. 2
- [11] Candelaria Mosquera, Luciana Ferrer, Diego H Milone, Daniel Luna, and Enzo Ferrante. Class imbalance on medical image classification: towards better evaluation practices for discrimination and calibration performance. *European Radiology*, 34(12):7895–7903, 2024. 2
- [12] Aditya Parikh, Sneha Das, and Aasa Feragen. Investigating label bias and representational sources of age-related disparities in medical segmentation, 2025. 1
- [13] Nina Weng, Siavash Bigdeli, Eike Petersen, and Aasa Fer-

agen. Are sex-based physiological differences the cause of gender bias for chest x-ray diagnosis? In *Workshop on clinical image-based procedures*, pages 142–152. Springer, 2023. 2

- [14] Ross Wightman. Pytorch image models. <https://github.com/rwightman/pytorch-image-models>, 2019. 3
- [15] Sierra Wyllie, Ilia Shumailov, and Nicolas Papernot. Fairness feedback loops: training on synthetic data amplifies bias. In *Proceedings of the 2024 ACM Conference on Fairness, Accountability, and Transparency*, pages 2113–2147, 2024. 1